ISSN 1990-7931, Russian Journal of Physical Chemistry B, 2025, Vol. 19, No. 3, pp. 722–736. © Pleiades Publishing, Ltd., 2025.

CHEMICAL PHYSICS OF NANOMATERIALS

Alkali Metals Doped on Tin-Silicon and Germanium-Silicon Oxides for Energy Storage in Hybrid Biofuel Cells: A First-Principles Study

F. Mollaamin*

Department of Biomedical Engineering, Faculty of Engineering and Architecture, Kastamonu University, Kastamonu, Turkey

**e-mail: fmollaamin@kastamonu.edu.tr*

Received January 14, 2025; revised February 13, 2025; accepted February 20, 2025

Abstract—Today, it is crucial to distinguish the potential of hydrogen technologies and bring up all perspectives of their performance, from technological progresses to economic and social effects. So long as Li-ion batteries have their difficulties, the demand to improve beyond lithium batteries goes beyond the issues of sustainability and safety. Therefore, in this article, it has been evaluated the promising alternative alkali metals of sodium-ion and potassium ion, batteries. A comprehensive investigation on hydrogen grabbing by LiNa[GeO–SiO], LiK[GeO–SiO], LiNa[SnO–SiO], and LiK[SnO–SiO] was carried out including using DFT computations at the "CAM–B3LYP–D3/6-311+G(*d*, *p*)" level of theory. The hypothesis of the hydrogen adsorption phenomenon was confirmed by density distributions of CDD, TDOS, and ELF for nanoclusters of LiNa[GeO–SiO]–$2H_2$, LiK[GeO–SiO]–$2H_2$, LiNa[SnO–SiO]–$2H_2$, and LiK[SnO–SiO]–$2H_2$. The fluctuation in charge density values demonstrates that the electronic densities were mainly located in the boundary of adsorbate/adsorbent atoms during the adsorption status. As the advantages of lithium, sodium or potassium over Ge,Sn/Si possess its higher electron and hole motion, allowing lithium, sodium or potassium instruments to operate at higher frequencies than Ge,Sn/Si instruments. Among these, sodium-ion batteries seem to show the most promise in terms of initial capacity.

Keywords: hydrogen adsorption, energy storage, sodium/potassium batteries, density of states, charge distribution

DOI: 10.1134/S1990793125700393

1. INTRODUCTION

Although lithium-ion batteries have become available in the current technology perspective through their high energy density, they face serious discussions in terms of safety and sustainability. With the enhancing global request for energy, there is an essential need for alternative efficient energy storage systems. This is driving research into non-lithium battery systems. This paper presents comprehensive research on non-lithium battery technologies, specifically sodium-ion and potassium-ion batteries [1–10].

Along with sodium ion, potassium-ion is the prime chemistry replacement candidate for lithium-ion batteries. Potassium-ion has certain advantages over similar lithium-ion such as: the cell design is simple, and both the material and the fabrication procedures are cheaper. The key advantage is the abundance and low cost of potassium in comparison with lithium, which makes potassium batteries a promising candidate for large scale batteries such as household energy storage and electric vehicles. Another advantage of a potassium-ion battery over a lithium-ion battery is potentially faster charging [11–20].

Recently, Si-, Ge- or Sn-carbide nanostructures have been suggested as engaged H-grabbing compounds. Since the polarizability of silicon is more than carbon, it is supposed that Si–C/Si nanosheet might attach to compositions more strongly in comparison to the net carbon nano-surfaces [21–31]. It was presented with a novel semiconducting alloy, silicon-tin (SiSn), as channel material for complementary metal oxide semiconductor (CMOS) circuit applications [32]. Nanomaterials with remarkable specific structures indicate promising applications in the field of energy storage, electrocatalysis, and fuel cells [33–40]. In our previous works, the investigation of energy storage in fuel cells through hydrogen adsorption has been accomplished using DFT calculations through different nanomaterials consisting of silicon/germanium/tin/lead nano-carbides [41], magnesium-aluminum alloy [42], aluminum/carbon/silicon doping boron nitride nanocage [43] and ternary aluminum gallium nitride and its doped derivatives with silicon, germanium, palladium and platinum [44].

Nanomaterials with remarkable specific structures indicate promising applications in the field of energy storage, electrocatalysis, and fuel cells. Currently, the present research aims to explore the possibility of

using LiNa[GeO–SiO], LiK[GeO–SiO], LiNa[SnO–SiO], and LiK[SnO–SiO] nanoclusters for hydrogen storage by employing first-principles calculations. We have analyzed the structural and electronic properties of LiNa[GeO–SiO], LiK[GeO–SiO], LiNa[SnO–SiO], and LiK[SnO–SiO] nanoclusters and hydrogen-adsorbed nanoclusters of LiNa[GeO–SiO]–$2H_2$, LiK[GeO–SiO]–$2H_2$, LiNa[SnO–SiO]–$2H_2$, and LiK[SnO–SiO]–$2H_2$ using state-of-the-art computational techniques. The development of high-energy density electrodes is necessary to assure a substantial energy output. Additionally, it is crucial to preserve structural stability through thoughtful material and electrode design to provide long-lasting cycle performance. To attain a substantial energy density and reliable cycling stability in sodium ion batteries (SIBs) or potassium ion batteries (PIBs), it is imperative to acquire a comprehensive understanding of the interfacial chemistry and ion diffusion within solid surface.

2. THEORY, MATERIALS AND COMPUTATION

With the pressure for renewable energy resources and the enchantingly digitalized current lifestyle, the need for batteries will augment. The aim of this study is to hydrogen adsorption by using alkali metals-based nanoclusters of LiNa[GeO–SiO], LiK[GeO–SiO], LiNa[SnO–SiO], and LiK[SnO–SiO] (Fig. 1) which can increase the hydrogen storage in cell batteries, transistors or other semiconductors. In our research, the calculations have been done by CAM–B3LYP–D3 /EPR–3 level of theory [45]. Figure 1 shows the process of hydrogen adsorption by LiNa[GeO–SiO], LiK[GeO–SiO], LiNa[SnO–SiO], and LiK[SnO–SiO] nanoclusters and hydrogen-adsorbed nanoclusters of LiNa[GeO–SiO]–$2H_2$, LiK[GeO–SiO]–$2H_2$, LiNa[SnO–SiO]–$2H_2$, and LiK[SnO–SiO]–$2H_2$. The Bader charge analysis [46, 47] was discussed during trapping of hydrogen atoms by LiNa[GeO–SiO], LiK[GeO–SiO], LiNa[SnO–SiO], and LiK[SnO–SiO] nanoclusters (Fig. 1). The rigid potential energy surface using density functional theory [48–61] was performed due to Gaussian 16 revision C.01 program package [62] and GaussView 6.1 [63]. The coordination input for hydrogen grabbing by LiNa[GeO–SiO], LiK[GeO–SiO], LiNa[SnO–SiO], and LiK[SnO–SiO] has been LANL2DZ and 6-311+G(d, p) basis sets.

3. RESULTS AND DISCUSSION

3.1. Charge Density Differences Analysis

The amounts of charge density differences (CDD) are measured by considering isolated atoms or noninteracting ones. The mentioned approximation can be the lightest to use because the superposition value may be received from the primary status of the self-consistency cycle in the code that carries out the density functional theory (Figs. 2a, 2a', 2b, 2b', 2c, 2c', 2d, 2d') [64].

In Fig. 2a, LiNa[GeO–SiO] cluster with the fluctuation in the region around –12 to +8 Bohr forms the nanocluster of LiNa[GeO–SiO]–$2H_2$ (Fig. 2a') in the area around –12 to +8 Bohr. Furthermore, the atoms of O2, O3, O7–O12, O14, O15, O17, O18, O22–O27, O29, O30 from LiK[GeO–SiO] (Fig. 2b) have shown the fluctuation around –12 to +8 Bohr towards formation of LiK[GeO–SiO]–$2H_2$ through hydrogen adsorption (Fig. 2b'). In addition, LiNa[SnO–SiO] cluster with the fluctuation in the region around –12 to +8 Bohr (Fig. 2c) forms the nanocluster of LiNa[SnO–SiO]–$2H_2$ during hydrogen grabbing (Fig. 2c') in the same range of area around –12 to +8 Bohr. Besides, LiK[SnO–SiO] cluster with the fluctuation in the region around –12 to +8 Bohr (Fig. 2d) forms the nanocluster of LiK[SnO–SiO]–$2H_2$ during hydrogen grabbing (Fig. 2d') in the same range of area around –12 to +8 Bohr.

Atomic charge was discussed during trapping of hydrogens by LiNa[GeO–SiO], LiK[GeO–SiO], LiNa[SnO–SiO], and LiK[SnO–SiO] nanoclusters towards formation of LiNa[GeO–SiO]–$2H_2$, LiK[GeO–SiO]–$2H_2$, LiNa[SnO–SiO]–$2H_2$, and LiK[SnO–SiO]–$2H_2$, respectively (Tables 1, 2).

The atomic charge of Si, Ge, Sn, O, and alkali metals of Li, Na, K and hydrogen atoms absorbed on LiNa[GeO–SiO], LiK[GeO–SiO], LiNa[SnO–SiO], and LiK[SnO–SiO] nanoclusters have been measured. The values detect that with adding lithium, sodium and potassium, the negative atomic charge of oxygen atoms of O2, O3, O7–O12, O14, O15, O17, O18, O22–O27, O29, O30 in LiNa[GeO–SiO], LiK[GeO–SiO], LiNa[SnO–SiO], and LiK[SnO–SiO] nanoclusters augments. In fact, LiNa[GeO–SiO], LiK[GeO–SiO], LiNa[SnO–SiO], and LiK[SnO–SiO] nanoclusters have shown more efficiency than [GeO–SiO] or [SnO–SiO] cluster [30] for admitting the electron from electron donor of H33, H34, H35 and H36 (Tables 1, 2).

The changes of charge density analysis in the adsorption process have illustrated that LiNa[GeO–SiO] has shown the "Bader charge" of –1.639 coulomb before hydrogen adsorption and –1.646 coulomb after hydrogen adsorption. Moreover, the changes of charge density analysis for LiK[GeO–SiO] has shown the "Bader charge" of –1.606 coulomb before hydrogen adsorption and –1.610 coulomb after hydrogen adsorption. LiNa[SnO–SiO] has shown the "Bader charge" of –1.833 coulomb before hydrogen adsorption and –1.845 coulomb after hydrogen adsorption. However, LiK[SnO–SiO] has shown the "Bader charge" of –1.723 coulomb before hydrogen adsorption and –1.743 coulomb after hydrogen adsorption. The differences of charge density for these structures are measured as: $\Delta Q_{\text{LiNa[GeO–SiO]}} = 0.007$,

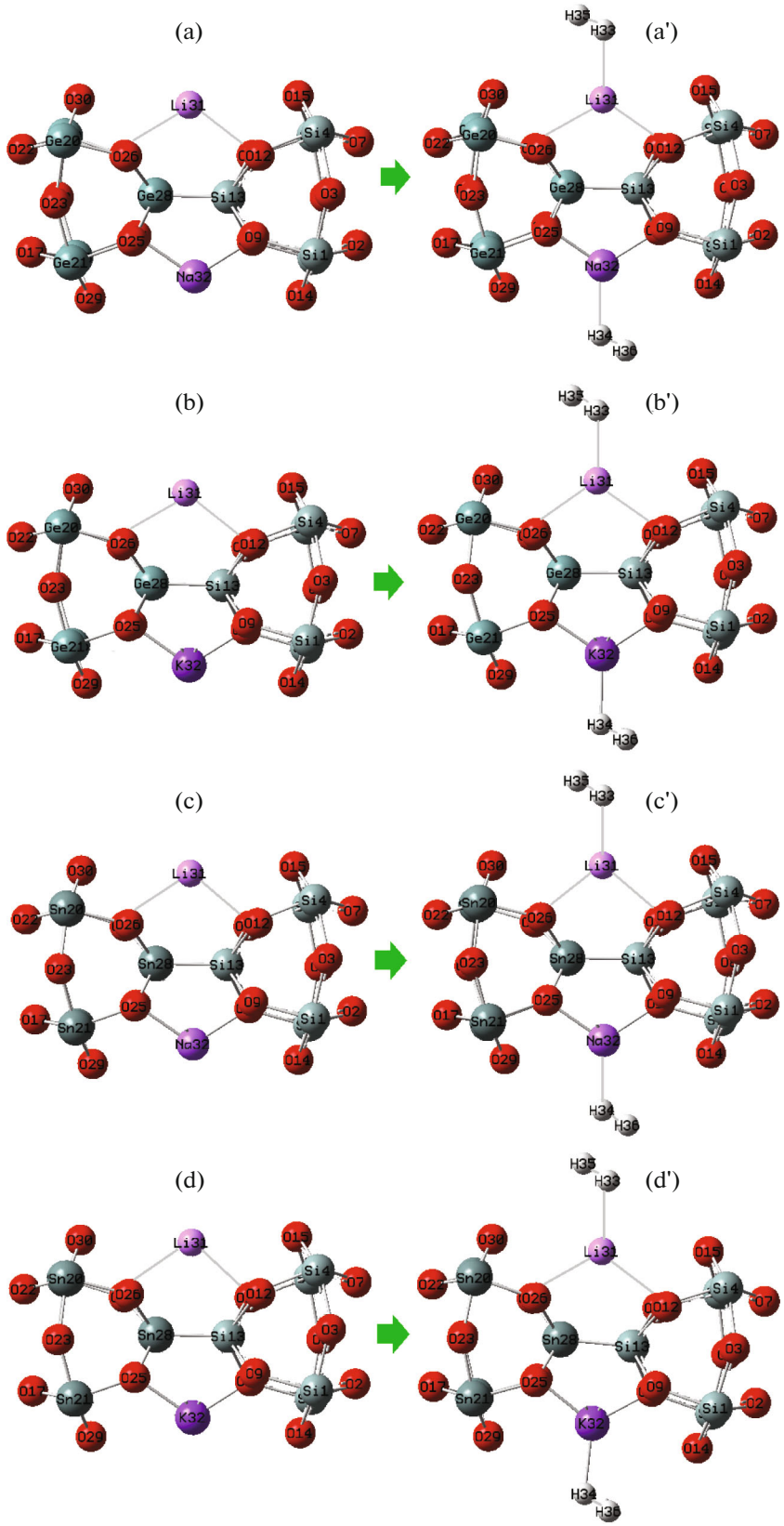

Fig. 1. Adding Li, Na, K to [GeO–SiO] and [SnO–SiO] nanoclusters and formation of (a) LiNa[GeO–SiO], (b) LiK[GeO–SiO], (c) LiNa[SnO–SiO], (d) LiK[SnO–SiO] nanoclusters towards energy storage through hydrogen adsorption as (a') LiNa[GeO–SiO]–$2H_2$, (b') LiK[GeO–SiO]–$2H_2$, (c') LiNa[SnO–SiO]–$2H_2$, (d') LiK[SnO–SiO]–$2H_2$ in novel batteries.

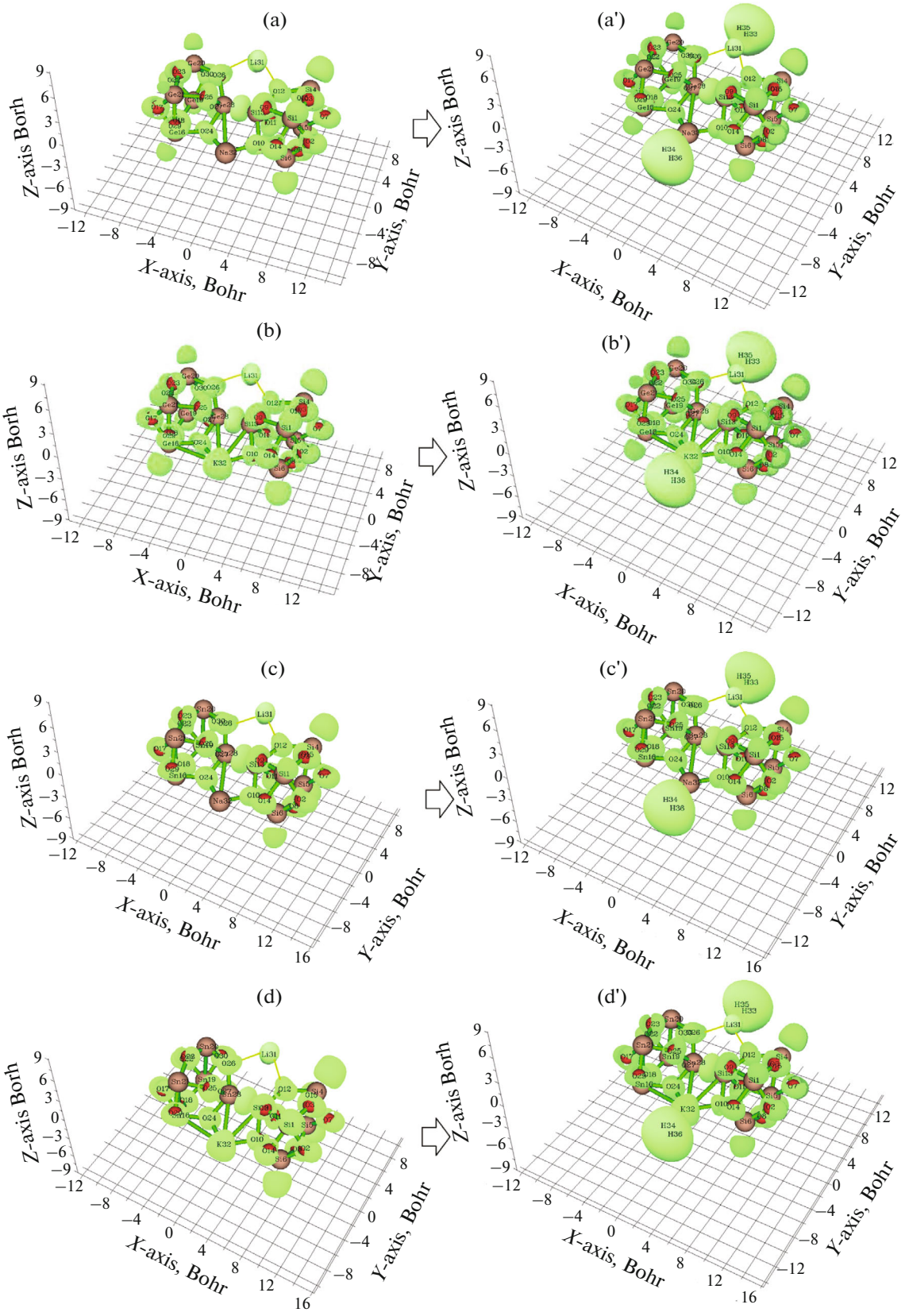

Fig. 2. CDD graphs for (a) LiNa[GeO–SiO], (a') LiNa[GeO–SiO]–$2H_2$, (b) LiK[GeO–SiO], (b') LiK[GeO–SiO]–$2H_2$, (c) LiNa[SnO–SiO], (c') LiNa[SnO–SiO]–$2H_2$, (d) LiK[SnO–SiO], (d') LiK[SnO–SiO]–$2H_2$ nanoclusters.

Table 1. The atomic charge (Q/coulomb) for LiNa[GeO–SiO], LiNa[GeO–SiO]–$2H_2$, LiK[GeO–SiO], LiK[GeO–SiO]–$2H_2$ nanoclusters

LiNa[GeO–SiO]		LiNa[GeO–SiO]–$2H_2$		LiK[GeO–SiO]		LiK[GeO–SiO]–$2H_2$	
atom	charge	atom	charge	atom	charge	atom	charge
Si1	1.46	Si1	1.46	Si1	1.46	Si1	1.47
O2	−0.65	O2	−0.66	O2	−0.70	O2	−0.63
O3	−0.83	O3	−0.83	O3	−0.83	O3	−0.83
Si4	1.43	Si4	1.43	Si4	1.43	Si4	1.43
Si5	1.45	Si5	1.45	Si5	1.461	Si5	1.44
Si6	1.46	Si6	1.46	Si6	1.45	Si6	1.47
O7	−0.68	O7	−0.68	O7	−0.65	O7	−0.71
O8	−0.84	O8	−0.84	O8	−0.83	O8	−0.83
O9	−0.79	O9	−0.79	O9	−0.79	O9	−0.80
O10	−1.00	O10	−0.99	O10	−1.06	O10	−1.05
O11	−0.80	O11	−0.80	O11	−0.80	O11	−0.80
O12	−0.95	O12	−0.95	O12	−0.94	O12	−0.96
Si13	1.64	Si13	1.64	Si13	1.60	Si13	1.61
O14	−0.73	O14	−0.73	O14	−0.71	O14	−0.76
O15	−0.72	O15	−0.72	O15	−0.76	O15	−0.69
Ge16	1.41	Ge16	1.42	Ge16	1.40	Ge16	1.40
O17	−0.65	O17	−0.65	O17	−0.67	O17	−0.60
O18	−0.78	O18	−0.78	O18	−0.78	O18	−0.78
Ge19	1.40	Ge19	1.40	Ge19	1.38	Ge19	1.38
Ge20	1.39	Ge20	1.39	Ge20	1.40	Ge20	1.37
Ge21	1.40	Ge21	1.40	Ge21	1.40	Ge21	1.40
O22	−0.66	O22	−0.66	O22	−0.62	O22	−0.69
O23	−0.78	O23	−0.78	O23	−0.78	O23	−0.79
O24	−0.96	O24	−0.95	O24	−1.00	O24	−0.99
O25	−0.78	O25	−0.78	O25	−0.79	O25	−0.78
O26	−0.91	O26	−0.90	O26	−0.91	O26	−0.91
O27	−0.78	O27	−0.78	O27	−0.76	O27	−0.78
Ge28	1.30	Ge28	1.29	Ge28	1.23	Ge28	1.24
O29	−0.74	O29	−0.74	O29	−0.70	O29	−0.7
O30	−0.72	O30	−0.72	O30	−0.73	O30	−0.67
Li31	0.74	Li31	0.63	Li31	0.73	Li31	0.64
Na32	0.71	Na32	0.63	K32	0.92	K32	0.87
		H33	−0.02			H33	−0.02
		H34	−0.01			H34	−0.04
		H35	0.12			H35	0.12
		H36	0.08			H36	0.06

Table 2. The atomic charge (Q/coulomb) for LiNa[SnO–SiO], LiNa[SnO–SiO]–$2H_2$, LiK[SnO–SiO], LiK[SnO–SiO]–$2H_2$ nanoclusters

LiNa[SnO–SiO]		LiNa[SnO–SiO]–$2H_2$		LiK[SnO–SiO]		LiK[SnO–SiO]–$2H_2$	
atom	charge	atom	charge	atom	charge	atom	charge
Si1	1.46	Si1	1.46	Si1	1.43	Si1	1.46
O2	–0.63	O2	–0.63	O2	–0.63	O2	–0.63
O3	–0.83	O3	–0.83	O3	–0.85	O3	–0.83
Si4	1.41	Si4	1.41	Si4	1.38	Si4	1.41
Si5	1.44	Si5	1.43	Si5	1.42	Si5	1.43
Si6	1.46	Si6	1.46	Si6	1.42	Si6	1.46
O7	–0.72	O7	–0.72	O7	–0.66	O7	–0.72
O8	–0.83	O8	–0.83	O8	–0.85	O8	–0.83
O9	–0.79	O9	–0.79	O9	–0.78	O9	–0.80
O10	–1.00	O10	–1.00	O10	–1.06	O10	–1.05
O11	–0.81	O11	–0.81	O11	–0.80	O11	–0.80
O12	–0.95	O12	–0.95	O12	–0.94	O12	–0.95
Si13	1.39	Si13	1.40	Si13	1.37	Si13	1.38
O14	–0.76	O14	–0.77	O14	–0.72	O14	–0.77
O15	–0.69	O15	–0.69	O15	–0.71	O15	–0.70
Sn16	1.69	Sn16	1.70	Sn16	1.69	Sn16	1.68
O17	–0.81	O17	–0.81	O17	–0.81	O17	–0.80
O18	–0.88	O18	–0.88	O18	–0.88	O18	–0.87
Sn19	1.69	Sn19	1.69	Sn19	1.70	Sn19	1.69
Sn20	1.67	Sn20	1.67	Sn20	1.67	Sn20	1.67
Sn21	1.69	Sn21	1.69	Sn21	1.70	Sn21	1.69
O22	–0.84	O22	–0.84	O22	–0.83	O22	–0.84
O23	–0.89	O23	–0.89	O23	–0.89	O23	–0.89
O24	–1.06	O24	–1.06	O24	–1.11	O24	–1.11
O25	–0.91	O25	–0.91	O25	–0.90	O25	–0.90
O26	–1.00	O26	–0.99	O26	–1.00	O26	–1.00
O27	–0.93	O27	–0.93	O27	–0.92	O27	–0.92
Sn28	1.83	Sn28	1.84	Sn28	1.72	Sn28	1.74
O29	–0.89	O29	–0.89	O29	–0.89	O29	–0.89
O30	–0.86	O30	–0.86	O30	–0.86	O30	–0.86
Li31	0.70	Li31	0.60	Li31	0.71	Li31	0.60
Na32	0.66	Na32	0.57	K32	0.89	K32	0.85
		H33	–0.02			H33	–0.02
		H34	–0.01			H34	–0.04
		H35	0.12			H35	0.12
		H36	0.08			H36	0.06

$\Delta Q_{LiK[GeO-SiO]} = 0.004$, $\Delta Q_{LiNa[SnO-SiO]} = 0.012$, $\Delta Q_{LiK[SnO-SiO]} = 0.02$ coulomb. Therefore, the results have shown that the cluster of LiK[SnO–SiO] and LiNa[SnO–SiO] may have the most tensity for electron accepting owing to hydrogen grabbing.

3.2. TDOS Analysis

Squirming the molecular orbital data owing to gaussian graphs of unit altitude and entire width at "full width at half maximum (FWHM)" of 0.3 eV by "GaussSum 3.0.2" [65] have computed total density of states (TDOS) diagrams. Regarding adsorption behavior of hydrogen by LiNa[GeO–SiO], LiK[GeO–SiO], LiNa[SnO–SiO], and LiK[SnO–SiO] nanoclusters, TDOS has been measured. This parameter can indicate the existence of important chemical interactions often on the convex side (Figs. 3a, 3a', 3b, 3b', 3c, 3c', 3d, 3d'). During formation of LiNa[GeO–SiO] cluster, Fig. 3a has shown sharp and sophisticated peaks around –0.3, –0.45 and –0.60 a.u. due to covalent bond between two atoms of Li and Na with [GeO–SiO] cluster. Moreover, LiNa[GeO–SiO]–$2H_2$ has indicated a duplicate peak around –0.45 to –0.5 a.u. during hydrogen adsorption (Fig. 3a'). LiK[GeO–SiO] cluster has shown pointed peaks around –0.3, –0.45 and –0.60 a.u. due to covalent bond between two atoms of Li and K with [GeO–SiO] cluster (Fig. 3b). Furthermore, LiK[GeO–SiO]–$2H_2$ has indicated a duplicate peak around –0.45 to –0.5 a.u. during hydrogen adsorption (Fig. 3b'). Furthermore, The maximum energy of TDOS for LiNa[SnO–SiO] (Fig. 3c) with several peaks around –0.30, –0.40, and –0.55 a.u. with maximum density of state of ≈24 around –0.30 a.u. has been shown. However, the TDOS curve for LiNa[SnO–SiO]–$2H_2$ (Fig. 3c') has shown two pointed peaks around –0.30 and –0.55 a.u. through some fluctuations in the behavior of the graphs. Similar behavior of TDOS graphs have been observed for hybrid cluster of LiK[SnO–SiO] (Fig. 3d) and its hydrogenation complex of LiK[SnO–SiO]–$2H_2$ (Fig. 3d') with several remarkable peaks around –0.30, –0.45, –0.55, and –0.7 a.u.

3.3. ELF Analysis

A type of scalar fields called electron localization function (ELF) may demonstrate a broad span of bonding samples. Nevertheless, the distinction between deduced/raised electron delocalization/localization into cyclic π-conjugated sets stays encouraging for ELF [66]. The grosser the electron localization is in an area, the more likely the electron movement is restricted within it. Therefore, they might be discerned from the ones away if electrons are totally centralized. As Bader investigated, the zones with large electron localization possess extensive magnitudes of Fermi hole integration [67]. But, with having a six-dimension function for the Fermi hole, it seems hard to be studied directly. Then, Becke and Edgecombe remarked that spherically averaged like spin conditional pair probability possesses a direct correlation with the Fermi hole and proposed the parameter of ELF in Multiwfn program [68, 69] and popularized for spin-polarized procedure [70]:

$$D_\sigma(r) = \tau_\sigma(r) - \frac{1}{4}\frac{(\nabla\rho_\sigma(r))^2}{\rho_\sigma(r)}, \quad (1)$$

where ρ is the electron spin density and τ the kinetic energy density. The second term is the bosonic kinetic energy density, so D is the contribution due to fermions. D is expected to be small in those regions of space where localized electrons are to be found. Given the arbitrariness of the magnitude of the localization measure provided by D, it is compared to the corresponding value for a uniform electron gas with spin density equal to ρ(r), which is given by

$$D_\sigma^0(r) = \frac{3}{5}\left(6\pi^2\right)^{2/3}\rho_\sigma^{5/3}(r), \quad (2)$$

and

$$\chi_\sigma(r) = \frac{D_\sigma(r)}{D_\sigma^0(r)}, \quad (3)$$

where $\chi_\sigma(r)$ is a dimensionless localization index that expresses electron localization for the uniform electron gas. And

$$\mathrm{ELF}(r) = \frac{1}{1+\chi_\sigma^2(r)}. \quad (4)$$

Regarding kinetic energy, ELF was rechecked to be more punctual for both Kohn–Sham DFT and post-HF wavefunctions [71]. Trapping of hydrogens by LiNa[GeO–SiO], LiK[GeO–SiO], LiNa[SnO–SiO], and LiK[SnO–SiO] nanoclusters towards formation of LiNa[GeO–SiO]–$2H_2$, LiK[GeO–SiO]–$2H_2$, LiNa[SnO–SiO]–$2H_2$, and LiK[SnO–SiO]–$2H_2$ can be defined by ELF graphs owing to exploring their delocalization/localization characterizations of electrons and chemical bonds (Figs. 4a, 4a', 4b, 4b', 4c, 4c', 4d, 4d').

A vaster jointed area engaged by an isosurface map has shown the electron delocalization in LiNa[GeO–SiO] (Fig. 4a), LiNa[GeO–SiO]–$2H_2$ (Fig. 4a'), LiK[GeO–SiO] (Fig. 4b), LiK[GeO–SiO]–$2H_2$ (Fig. 4b'), LiNa[SnO–SiO] (Fig. 4c), LiNa[SnO–SiO]–$2H_2$ (Fig. 4c'), LiK[SnO–SiO] (Fig. 4d), and LiK[SnO–SiO]–$2H_2$ (Fig. 4d') through labeling atoms of O12, Si13, O26, Ge28/Sn28, X31 (X=Li, Na or K) and H35. In fact, the counter map of ELF can

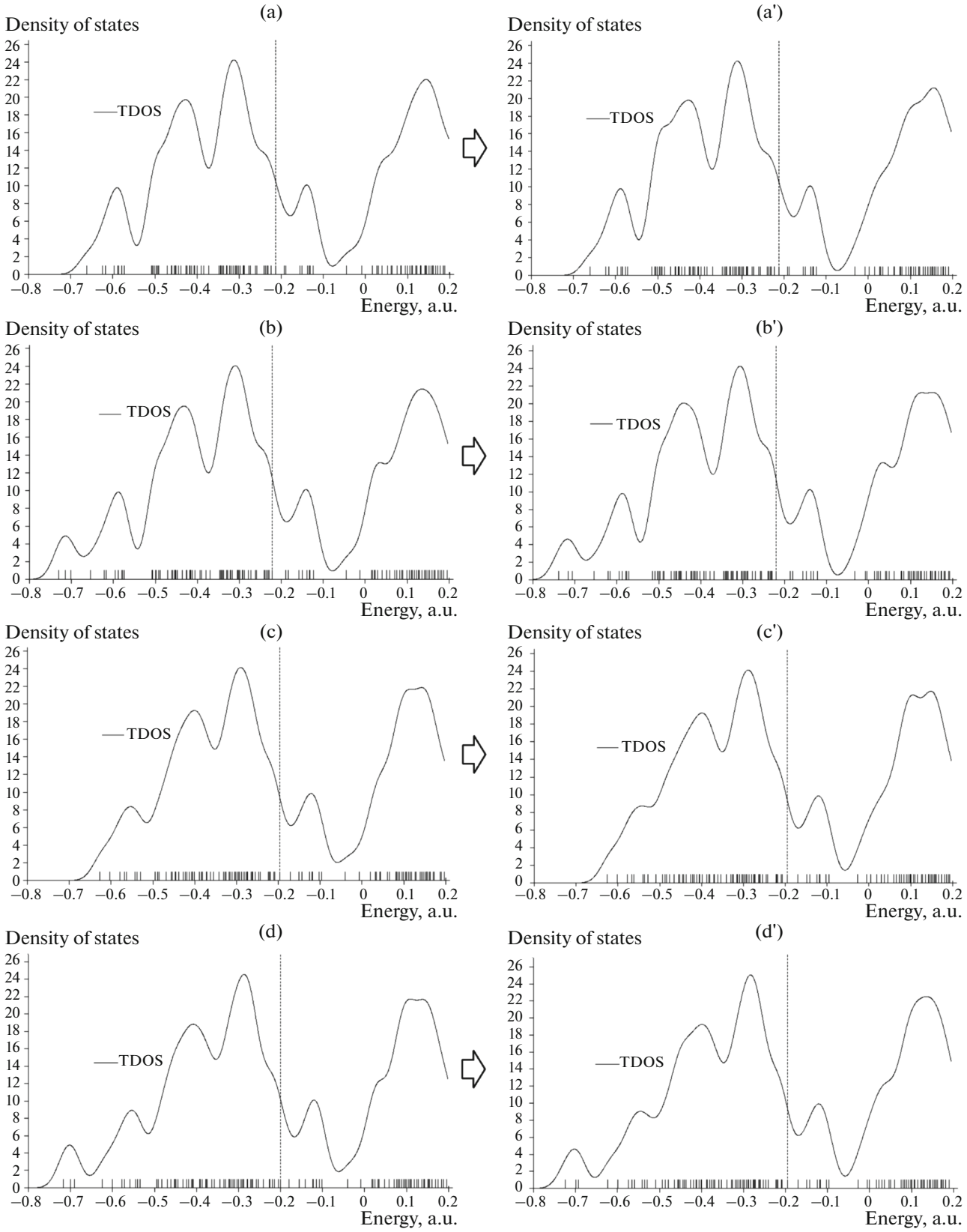

Fig. 3. TDOS graphs of (a) LiNa[GeO–SiO], (a') LiNa[GeO–SiO]–$2H_2$, (b) LiK[GeO–SiO], (b') LiK[GeO–SiO]–$2H_2$, (c) LiNa[SnO–SiO], (c') LiNa[SnO–SiO]–$2H_2$, (d) LiK[SnO–SiO], (d') LiK[SnO–SiO]–$2H_2$ nanoclusters.

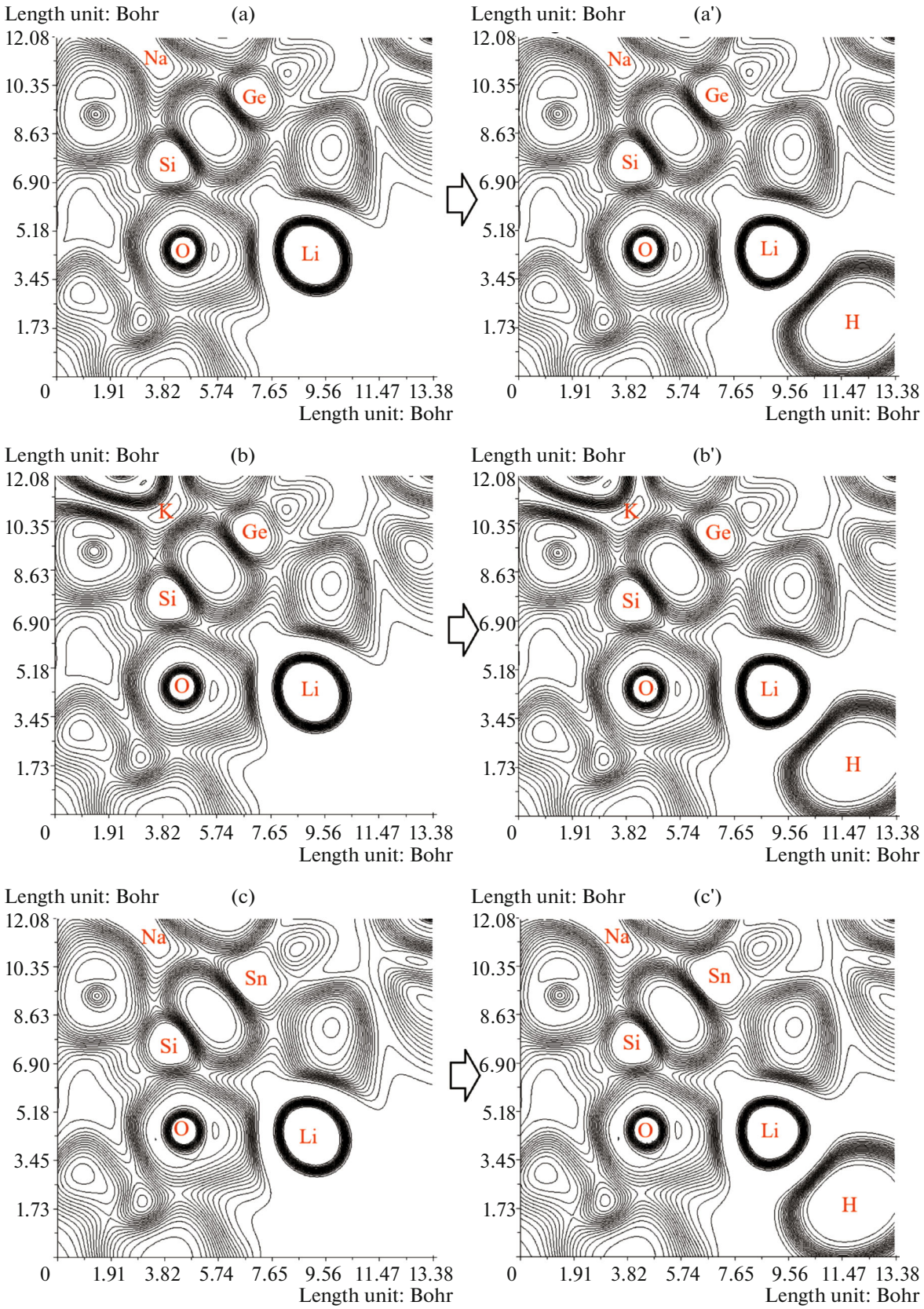

Fig. 4. The counter map of ELF graphs for (a) LiNa[GeO–SiO], (a') LiNa[GeO–SiO]–$2H_2$, (b) LiK[GeO–SiO], (b') LiK[GeO–SiO]–$2H_2$, (c) LiNa[SnO–SiO], (c') LiNa[SnO–SiO]–$2H_2$, (d) LiK[SnO–SiO], (d') LiK[SnO–SiO]–$2H_2$ nanoclusters.

Table 3. Dipole moment (debye), LUMO, HOMO, and energy gap (ΔE) for LiNa[GeO–SiO], LiK[GeO–SiO], LiNa[SnO–SiO], and LiK[SnO–SiO] through hydrogen grabbing and formation of LiNa[GeO–SiO]–$2H_2$, LiK[GeO–SiO]–$2H_2$, LiNa[SnO–SiO]–$2H_2$, and LiK[SnO–SiO]–$2H_2$ heteroclusters

Heteroclusters	Dipole moment, D	E_{HOMO}, eV	E_{LUMO}, eV	$\Delta E = E_{LUMO} - E_{HOMO}$, eV
LiNa[GeO–SiO]	2.08	–5.80	–5.26	0.54
LiNa[GeO–SiO]–$2H_2$	2.28	–5.76	–5.22	0.54
LiK[GeO–SiO]	1.56	–6.03	–5.14	0.88
LiK[GeO–SiO]–$2H_2$	1.86	–6.02	–5.08	0.93
LiNa[SnO–SiO]	5.07	–5.34	–4.67	0.66
LiNa[SnO–SiO]–$2H_2$	5.18	–5.30	–4.64	0.66
LiK[SnO–SiO]	6.47	–5.46	–4.90	0.56
LiK[SnO–SiO]–$2H_2$	5.28	–5.33	–4.62	0.70

confirm that LiNa[GeO–SiO], LiK[GeO–SiO], LiNa[SnO–SiO], LiK[SnO–SiO] nanoclusters may increase the efficiency during hydrogen adsorption towards formation of LiNa[GeO–SiO]–$2H_2$, LiK[GeO–SiO]–$2H_2$, LiNa[SnO–SiO]–$2H_2$, and LiK[SnO–SiO]–$2H_2$. In fact, it can be proposed a cell battery model that bridges the energy density and rate capability between that of supercapacitors or pseudocapacitors with that of traditional lithium-ion batteries. This is accomplished by pairing an anode that enables ion co-intercalation and an open framework cathode that sustains cell-level stability and high-rate performance. The sodium or potassium storage processes, the evolution of sodium ion batteries (SIBs) or potassium ion batteries (PIBs), and the benefits and drawbacks of each material group are all covered.

Moreover, intermolecular orbital overlap integral is important in discussions of intermolecular charge transfer which can calculate HOMO–HOMO and LUMO–LUMO overlap integrals between the H_2 molecules and heteroclusters of LiNa[GeO–SiO], LiK[GeO–SiO], LiNa[SnO–SiO], LiK[SnO–SiO]. The applied wavefunction level is CAM–B3LYP–D3/6–311+G(d, p) that corresponds to HOMO and LUMO, respectively (Table 3).

The amount of "Mayer bond order" [72] is generally according to empirical bond order for the single bond is nearly 1.0. "Mulliken bond order" [73] with a small accord with empirical bond order is not appropriate for quantifying bonding strength, for which Mayer bond order always performs better. However, "Mulliken bond order" is a good qualitative indicator for "positive amount" of bonding and "negative amount" of antibonding which are evacuated and localized, respectively (Tables 4, 5).

As it is seen in Tables 4, 5, "Laplacian bond order" [74] has a straight cohesion with bond polarity, bond dissociation energy and bond vibrational frequency. The low value of Laplacian bond order might demonstrate that it is insensitive to the calculation degree applied for producing electron density. Generally, the value of "Fuzzy bond order" is near Mayer bond order, especially for low-polar bonds, but much more stable with respect to the change in basis-set. Computation of "Fuzzy bond order" demands running "Becke's DFT" numerical integration, owing to which the calculation value is larger than assessment of "Mayer bond order" and it can concede more precisely [75, 76]. The Fuzzy bond order close to ≈1 for hydrogenated heteroclusters containing LiNa[GeO–SiO]–$2H_2$, LiK[GeO–SiO]–$2H_2$, LiNa[SnO–SiO]–$2H_2$, and LiK[SnO–SiO]–$2H_2$ extracted from Tables5 show that hydrogen atoms can interact with surface of LiNa[GeO–SiO], LiK[GeO–SiO], LiNa[SnO–SiO], LiK[SnO–SiO] heteroclusters to form stable out-sphere adsorption complexes via hydrogen bonds and inner-sphere complexes via coordination bonds with the latter ones more stable. During the current state of the art, it has been examined in detail the prospective electrode materials of sodium and potassium combined with lithium and the underlying charge storage through hydrogen adsorption.

Table 4. The bond order of Mayer, Wiberg, Mulliken, Laplacian and Fuzzy from mixed alpha and beta density matrix for LiNa[GeO–SiO], LiK[GeO–SiO], LiNa[SnO–SiO], LiK[SnO–SiO] heteroclusters

Compound	Bond type	Bond order				
		Mayer	Wiberg	Mulliken	Laplacian	Fuzzy
LiNa[GeO–SiO]	O12–Si13	0.49	0.61	0.19	0.21	1.01
	O12–Li31	0.14	0.20	0.13	0.16	0.13
	O26–Li31	0.21	0.27	0.18	0.20	0.18
	O26–Ge28	0.64	0.57	0.24	0.24	1.04
	Si13–Ge28	0.63	0.75	0.68	2.28	0.83
	O10–Si13	0.43	0.60	0.12	0.14	0.91
	O10–Na32	0.24	0.22	0.26	0.07	0.63
	O24–Na32	0.24	0.22	0.27	0.05	0.56
	O24–Ge28	0.36	0.55	0.08	0.25	0.95
LiK[GeO–SiO]	O12–Si13	0.50	0.62	0.20	0.22	1.02
	O12–Li31	0.14	0.20	0.12	0.13	0.13
	O26–Li31	0.21	0.27	0.18	0.19	0.18
	O26–Ge28	0.50	0.58	0.26	0.24	1.05
	Si13–Ge28	0.70	0.78	0.54	2.36	0.85
	O10–Si13	0.43	0.59	0.08	0.13	0.90
	O10–K32	0.75	0.26	0.56	0.15	0.73
	O24–K32	0.75	0.25	0.46	0.11	0.65
	O24–Ge28	0.38	0.55	0.41	0.18	0.94
LiNa[SnO–SiO]	O12–Si13	0.49	0.60	0.18	0.20	1.00
	O12–Li31	0.15	0.21	0.13	0.16	0.13
	O26–Li31	0.24	0.28	0.20	0.14	0.15
	O26–Sn28	0.45	0.53	0.25	0.46	1.20
	Si13–Sn28	0.70	0.74	1.18	2.79	0.87
	O10–Si13	0.47	0.60	0.18	0.14	0.90
	O10–Na32	0.26	0.22	0.30	0.07	0.63
	O24–Na32	0.27	0.22	0.29	0.05	0.50
	O24–Sn28	0.32	0.18	0.11	0.41	1.11
LiK[SnO–SiO]	O12–Si13	0.50	0.61	0.18	0.21	1.01
	O12–Li31	0.15	0.20	0.14	0.15	0.13
	O26–Li31	0.24	0.28	0.20	0.14	0.15
	O26–Sn28	0.46	0.53	0.26	0.45	1.20
	Si13–Sn28	0.75	0.76	1.08	2.81	0.87
	O10–Si13	0.45	0.60	0.13	0.13	0.90
	O10–K32	0.17	0.26	0.54	0.15	0.72
	O24–K32	0.16	0.25	0.47	0.07	0.58
	O24–Sn28	0.36	0.52	0.08	0.39	1.10

Table 5. The bond order of Mayer, Wiberg, Mulliken, Laplacian and Fuzzy from mixed alpha and beta density matrix for LiNa[GeO–SiO]–$2H_2$, LiK[GeO–SiO]–$2H_2$, LiNa[SnO–SiO]–$2H_2$, LiK[SnO–SiO]–$2H_2$ heteroclusters

Compound	Bond type	Bond order				
		Mayer	Wiberg	Mulliken	Laplacian	Fuzzy
LiNa[GeO–SiO]–$2H_2$	O12–Si13	0.50	0.61	0.18	0.21	1.01
	O12–Li31	0.14	0.20	0.13	0.11	0.13
	O26–Li31	0.21	0.27	0.19	0.16	0.17
	O26–Ge28	0.47	0.57	0.24	0.24	1.04
	Si13–Ge28	0.63	0.75	0.70	2.28	0.83
	O10–Si13	0.43	0.60	0.11	0.14	0.91
	O10–Na32	0.26	0.22	0.28	0.07	0.63
	O24–Na32	0.25	0.22	0.28	0.05	0.56
	O24–Ge28	0.35	0.55	0.08	0.20	0.95
	Li31–H33	0.10	0.18	0.09	0.26	0.21
	Na32-H34	0.08	0.16	0.07	0.26	0.20
LiK[GeO–SiO]–$2H_2$	O12–Si13	0.48	0.60	0.18	0.20	1.01
	O12–Li31	0.14	0.21	0.13	0.20	0.13
	O26–Li31	0.22	0.27	0.19	0.14	0.18
	O26–Ge28	0.57	0.57	0.23	0.23	1.04
	Si13–Ge28	0.70	0.78	0.56	2.37	0.85
	O10–Si13	0.43	0.60	0.08	0.13	0.90
	O10–K32	0.16	0.26	0.55	0.15	0.72
	O24–K32	0.16	0.25	0.44	0.10	0.64
	O24–Ge28	0.39	0.56	0.06	0.20	0.95
	Li31–H33	0.10	0.18	0.10	0.19	0.21
	K32-H34	0.06	0.17	0.12	0.17	0.20
LiNa[SnO–SiO]–$2H_2$	O12–Si13	0.48	0.60	0.17	0.20	1.00
	O12–Li31	0.16	0.21	0.14	0.15	0.13
	O26–Li31	0.25	0.28	0.20	0.18	0.15
	O26–Sn28	0.62	0.53	0.25	0.45	1.20
	Si13–Sn28	0.70	0.74	1.20	2.79	0.87
	O10–Si13	0.46	0.60	0.17	0.14	0.91
	O10–Na32	0.27	0.22	0.30	0.07	0.62
	O24–Na32	0.28	0.22	0.30	0.05	0.49
	O24–Sn28	0.32	0.52	0.10	0.41	1.11
	Li31–H33	0.10	0.18	0.09	0.16	0.20
	Na32-H34	0.08	0.16	0.08	0.16	0.20
LiK[SnO–SiO]–$2H_2$	O12–Si13	0.49	0.60	0.18	0.20	1.00
	O12–Li31	0.16	0.21	0.14	0.19	0.13
	O26–Li31	0.25	0.28	0.20	0.17	0.15
	O26–Sn28	0.45	0.53	0.26	0.45	1.20
	Si13–Sn28	0.73	0.75	1.12	2.79	0.86
	O10–Si13	0.45	0.60	0.13	0.13	0.90
	O10–K32	0.16	0.26	0.53	0.15	0.72
	O24–K32	0.15	0.25	0.47	0.07	0.58
	O24–Sn28	0.37	0.52	0.08	0.39	1.10
	Li31–H33	0.10	0.17	0.09	0.22	0.20
	K32-H34	0.07	0.17	0.09	0.21	0.20

CONCLUSIONS

The large-scale energy storage in the form of SIBs or PIBs can be a hope in the future for a type of rechargeable battery. To attain a substantial energy density and reliable cycling stability in SIBs or PIBs, it is imperative to acquire a comprehensive understanding of the interfacial chemistry and ion diffusion within solid surface. H-grabbing by the nanoclusters of LiNa[GeO–SiO], LiK[GeO–SiO], LiNa[SnO–SiO], LiK[SnO–SiO] was investigated by first-principles computations of DFT method. The results have shown that the cluster of LiK[SnO–SiO] and LiNa[SnO–SiO] may have the most tensity for electron accepting owing to hydrogen grabbing. Moreover, hydrogen bond (H-bond) accepting sites by LiNa[GeO–SiO], LiK[GeO–SiO], LiNa[SnO–SiO], LiK[SnO–SiO] can alleviate parasitic hydrogen evolution in aqueous electrolytes in lithium, sodium, or potassium-ion batteries. The Fuzzy bond order close to ≈1 for hydrogenated heteroclusters have illustrated that hydrogen atoms can interact with surface of LiNa[GeO–SiO], LiK[GeO–SiO], LiNa[SnO–SiO], LiK[SnO–SiO] heteroclusters to form stable out-sphere adsorption complexes via hydrogen bonds and inner-sphere complexes via coordination bonds with the latter ones more stable.

ACKNOWLEDGMENTS

In successfully completing this paper and its research, the authors are grateful to Kastamonu University.

FUNDING

This work was supported by ongoing institutional funding. No additional grants to carry out or direct this particular research were obtained.

CONFLICT OF INTEREST

The author of this work declares that he has no conflicts of interest.

REFERENCES

1. E. N. Antonov, A. G. Ivanova, L. I. Krotova, et al., Russ. J. Phys. Chem. B **17**, 1555–1560 (2023). https://doi.org/10.1134/S199079312308002X
2. F. Mollaamin, Russ. J. Phys. Chem. B **18**, 805–820 (2024). https://doi.org/10.1134/S1990793124700131
3. F. Mollaamin, J. Comput. Theor. Nanosci. **11**, 2393–2398 (2014). https://doi.org/10.1166/jctn.2014.3653
4. F. Mollaamin, S. Mohammadi, Z. Khalaj, et al., Russ. J. Phys. Chem. B **18**, 67–82 (2024). https://doi.org/10.1134/S1990793124010330
5. V. Y. Agroskin, B. G. Bravy, G. K. Vasiliev, et al., Russ. J. Phys. Chem. B **17**, 1265–1269 (2023). https://doi.org/10.1134/S1990793123060131
6. A. Tahan, F. Mollaamin, and M. Monajjemi, Russ. J. Phys. Chem. A **83**, 587–597 (2009). https://doi.org/10.1134/S003602440904013X
7. S. Shahriari, M. Monajjemi, and F. Mollaamin, J. Chil. Chem. Soc. **67**, 5468–5476 (2022). https://doi.org/10.4067/S0717-97072022000205468
8. A. M. Tereza, G. L. Agafonov, E. K. Anderzhanov, et al., Russ. J. Phys. Chem. B **17**, 1294–1299 (2023). https://doi.org/10.1134/S1990793123060246
9. V. I. Petinov, V. M. Timin, K. V. Bozhenko, et al., Russ. J. Phys. Chem. B **18**, 365–368 (2024). https://doi.org/10.1134/S1990793124020301
10. A. M. Tereza, G. L. Agafonov, E. K. Anderzhanov, et al., Russ. J. Phys. Chem. B **17**, 974–978 (2023). https://doi.org/10.1134/S1990793123040309
11. M. A. A. Zadeh, H. Lari, L. Kharghanian, et al., J. Comput. Theor. Nanosci. **12**, 4358 (2015). https://doi.org/10.1166/jctn.2015.4366
12. E. I. Rudenko, N. V. Dohlikova, A. K. Gatin, et al., Russ. J. Phys. Chem. B **17**, 845–852 (2023). https://doi.org/10.1134/S1990793123040164
13. E. M. Sarasia, S. Afsharnezhad, B. Honarparvar, et al., Phys. Chem. Liq. **49**, 561–571 (2011). https://doi.org/10.1080/00319101003698992
14. M. Monajjemi, H. Yamola, and F. Mollaamin, Fulleren Nanotubes Carbon Nanostruct. **22**, 595–603 (2014). https://doi.org/10.1080/1536383X.2012.702163
15. F. Mollaamin, F. Najafi, M. Khaleghian, B. Khalili Hadad, and M. Monajjemi, Fulleren Nanotubes Carbon Nanostruct. **19**, 653–667 (2011). https://doi.org/10.1080/1536383X.2010.504956
16. S. Shahriari, M. Monajjemi, and K. Zare, Biointerface Res. Appl. Chem. **8**, 3219–3223 (2018).
17. R. R. Kayumov, A. P. Radaeva, A. A. Krupina, et al., Russ. J. Phys. Chem. B **17**, 801–809 (2023). https://doi.org/10.1134/S1990793123040097
18. F. Mollaamin and M. Monajjemi, Sensor Rev. **43**, 266–279 (2023). https://doi.org/10.1108/SR-03-2023-0040
19. K. Y. Troshin, N. M. Rubtsov, G. I. Tsvetkov, et al., Russ. J. Phys. Chem. B **17**, 979–985 (2023). https://doi.org/10.1134/S1990793123040310
20. K. Y. Troshin, N. M. Rubtsov, G. I. Tsvetkov, et al., Russ. J. Phys. Chem. B **17**, 433–438 (2023). https://doi.org/10.1134/S1990793123020185
21. Q. Q. Xiong, Russ. J. Phys. Chem. B **18**, 638–644 (2024). https://doi.org/10.1134/S1990793124700155
22. F. Mollaamin and M. Monajjemi, J. Comput. Theor. Nanosci. **12**, 1030–1039 (2015). https://doi.org/10.1166/jctn.2015.3846
23. X. Yuan, X. Tan, and B. Liu, Russ. J. Phys. Chem. B **17**, 886–895 (2023). https://doi.org/10.1134/S1990793123040322
24. L. I. Trakhtenberg, Russ. J. Phys. Chem. B **17**, 600–607 (2023). https://doi.org/10.1134/S1990793123030144

25. K. Bakhshi, F. Mollaamin, and M. Monajjemi, J. Comput. Theor. Nanosci. **8**, 763–768 (2011). https://doi.org/10.1166/jctn.2011.1750
26. F. Mollaamin and M. Monajjemi, Computation **11**, 108 (2023). https://doi.org/10.3390/computation11060108
27. M. Monajjemi, M. Khaleghian, N. Tadayonpour, et al., Int. J. Nanosci. **09**, 517–529 (2010). https://doi.org/10.1142/S0219581X10007071
28. F. Mollaamin and M. Monajjemi, J. Cluster Sci. **34**, 2901–2918 (2023). https://doi.org/10.1007/s10876-023-02436-5
29. N. Yodsin, H. Sakagami, T. Udagawa, et al., Mol. Catal. **504**, 111486 (2021). . https://doi.org/10.1016/j.mcat.2021.111486
30. A. E. Galashev, Russ. J. Phys. Chem. B **17**, 113–121 (2023). https://doi.org/10.1134/S1990793123010190
31. T. Wei, Y. Zhou, C. Sun, et al., Nano Res. **17**, 2763–2769 (2024). https://doi.org/10.1007/s12274-023-6187-8
32. K. Yao, M. Ling, G. Liu, et al., J. Phys. Chem. Lett. **9**, 5130–5134 (2018). https://doi.org/10.1021/acs.jpclett.8b02066
33. U. Cardella, L. Decker, J. Sundberg, et al., Int. J. Hydrogen Energy **42**, 12339–12354 (2017). https://doi.org/10.1016/j.ijhydene.2017.03.167
34. A. Hammad and I. Dincer, Int. J. Hydrogen Energy **43**, 1139–1151 (2018). https://doi.org/10.1016/j.ijhydene.2017.10.158
35. V. M. Azriel', V. M. Akimov, E. V. Ermolova, et al., Russ. J. Phys. Chem. B **18**, 1462–1472 (2024). https://doi.org/10.1134/S1990793124701409
36. M. A. Qyyum, Y. D. Chaniago, W. Ali, et al., Energies **13**, 5023 (2020). https://doi.org/10.3390/en13195023
37. A. H. Davtyan, Z. H. Manukyan, S. D. Arsentev, et al. Russ. J. Phys. Chem. B **18**, 461–467 (2024). https://doi.org/10.1134/S1990793124020209
38. X. Yu, X. Zhang, H. Wang, et al., J. Phys. Chem. C **121**, 22081– 22091 (2017). https://doi.org/10.1021/acs.jpcc.7b06361
39. F. Mollaamin and M. Monajjemi, J. Mol. Model. **29**, 119 (2023). https://doi.org/10.1007/s00894-023-05526-3
40. E. Rivard, M. Trudeau, K. Zaghib, Materials **12**, 1973 (2019). https://doi.org/10.3390/ma12121973
41. F. Mollaamin and M. Monajjemi, Russ. J. Phys. Chem. B **17**, 658–672 (2023). https://doi.org/10.1134/S1990793123030223
42. F. Mollaamin and Monajjemi, M. Russ. J. Phys. Chem. B **18**, 607–623 (2024). https://doi.org/10.1134/S1990793124020271
43. F. Mollaamin, S. Shahriari, and Monajjemi, M. Russ. J. Phys. Chem. B **18**, 398–418 (2024). https://doi.org/10.1134/S199079312402026X
44. F. Mollaamin and M. Monajjemi, Computation **12**, 234 (2024). https://doi.org/10.3390/computation12120234
45. T. Yanai, D. P. Tew, and N. C. Handy, Chem. Phys. Lett. **393**, 51–57 (2004). https://doi.org/10.1016/j.cplett.2004.06.011
46. G. Henkelman, A. Arnaldsson, and H. Jónsson, Comput. Mater. Sci. **36**, 354–360 (2006). https://doi.org/10.1016/j.commatsci.2005.04.010
47. F. Mollaamin and M. Monajjemi, J. Mol. Model. **29**, 170 (2023). https://doi.org/10.1007/s00894-023-05567-8
48. F. Mollaamin and M. Monajjemi, Russ. J. Phys. Chem. B **18**, 533–548 (2024). https://doi.org/10.1134/S199079312402012X
49. B. Khalili Hadad, F. Mollaamin, M. Monajjemi, Russ. Chem. Bull. **60**, 238–241 (2011). https://doi.org/10.1007/s11172-011-0039-5
50. F. Mollaamin and M. Monajjemi, C—J. Carbon Res. **9**, 20 (2023). https://doi.org/10.3390/c9010020
51. M. Monajjemi, F. Mollaamin, and S. Shojaei, Biointerface Res. Appl. Chem. **10**, 5575 (2020). https://doi.org/10.33263/BRIAC103.575585
52. F. Mollaamin and M. Monajjemi, Comput. Theor. Chem. **1237**, 114666 (2024). https://doi.org/10.1016/j.comptc.2024.114666
53. S. Shahriari, F. Mollaamin, and M. Monajjemi, Micromachines **14**, 241 (2023). https://doi.org/10.3390/mi14020241
54. F. Mollaamin and M. Monajjemi, J. Mol. Struct. **1300**, 137214 (2024). https://doi.org/10.1016/j.molstruc.2023.137214
55. F. Mollaamin, A. Ilkhani, N. Sakhaei, et al., J. Comput. Theor. Nanosci. **12**, 3148–3154 (2015). https://doi.org/10.1166/jctn.2015.4092
56. F. Mollaamin and M. Monajjemi, Sensor Rev. **44**, 179–193 (2024). https://doi.org/10.1108/SR-01-2024-0066
57. M. Monajjemi, L. Mahdavian, F. Mollaamin, et al., Russ. J. Inorg. Chem. **54**, 1465–1473 (2009). https://doi.org/10.1134/S0036023609090216
58. F. Mollaamin and M. Monajjemi, Russ. J. Phys. Chem. B **18**, 49–66 (2024). https://doi.org/10.1134/S1990793124010159
59. F. Mollaamin and M. Monajjemi, Int. J. Quantum Chem. **124**, e27348 (2024). https://doi.org/10.1002/qua.27348
60. F. Mollaamin and M. Monajjemi, Mol. Simul. **49**, 365–376 (2023). https://doi.org/10.1080/08927022.2022.2159996
61. S. V. Feskov, Russ. J. Phys. Chem. B **18**, 1–8 (2024). https://doi.org/10.1134/S1990793124010081
62. M. J. Frisch, G. W. Trucks, H. B. Schlegel, G. E. Scuseria, M. A. Robb, J. R. Cheeseman, G. Scalmani, V. Barone, G. A. Petersson, H. Nakatsuji, X. Li, M. Caricato, A. V. Marenich, J. Bloino, B. G. Janesko, R. Gomperts, B. Mennucci, H. P. Hratchian, J. V. Ortiz, A. F. Izmaylov, J. L. Sonnenberg, D. Williams-Young, F. Ding, F. Lipparini, F. Egidi, J. Goings, B. Peng, A. Petrone, T. Henderson, D. Ranasinghe, V. G. Zakrzewski, J. Gao, N. Rega, G. Zheng, W. Liang, M. Hada, M. Ehara, K. Toyota, R. Fukuda, J. Hasegawa, M. Ishida, T. Nakajima, Y. Honda, O. Kitao,

H. Nakai, T. Vreven, K. Throssell, J. A. Montgomery, Jr., J. E. Peralta, F. Ogliaro, M. J. Bearpark, J. J. Heyd, E. N. Brothers, K. N. Kudin, V. N. Staroverov, T. A. Keith, R. Kobayashi, J. Normand, K. Raghavachari, A. P. Rendell, J. C. Burant, S. S. Iyengar, J. Tomasi, M. Cossi, J. M. Millam, M. Klene, C. Adamo, R. Cammi, J. W. Ochterski, R. L. Martin, K. Morokuma, O. Farkas, J. B. Foresman, and D. J. Fox, *Gaussian 16, Revision C.01* (Gaussian, Inc., Wallingford, CT, 2016).

63. R. Dennington, T. A. Keith, and J. M. Millam, *GaussView, Version 6.06.16* (Semichem Inc., Shawnee Mission, KS, 2016).
64. Z. Xu, C. Qin, Y. Yu, et al., AIP Adv. **14**, 055114 (2024). https://doi.org/10.1063/5.0208082
65. N. M. O'Boyle, A. L. Tenderholt, and K. M. Langner, J. Comp. Chem. **29**, 839–845 (2008). https://doi.org/10.1002/jcc.20823
66. C. F. Matta, P. W. Ayers, and R. Cook, "The physics of electron localization and delocalization," in *Electron Localization-Delocalization Matrices*, Lecture Notes in Chemistry, Vol. 112 (Springer, Cham, 2024). https://doi.org/10.1007/978-3-031-51434-0_2
67. R. F. W. Bader, Theor. Chem. Acc. **105**, 276–283 (2001). https://doi.org/10.1007/s002140000233
68. T. Lu and F. Chen, J. Comput. Chem. **33**, 580–592 (2012). https://doi.org/10.1002/jcc.22885
69. T. Lu, J. Chem. Phys. **161**, 082503 (2024). https://doi.org/10.1063/5.0216272
70. A. D. Becke and K. E. Edgecombe, J. Chem. Phys. **92**, 5397–5403 (1990). https://doi.org/10.1063/1.458517
71. A. Savin, O. Jepsen, J. Flad, et al., Angew. Chem. Int. Ed. **31**, 187–188 (1992). https://doi.org/10.1002/anie.199201871
72. I. Mayer, Chem. Phys. Lett. **544**, 83–86 (2012). https://doi.org/10.1016/j.cplett.2012.07.0
73. F. Mollaamin, S. Shahriari, M. Monajjemi, et al., J. Cluster Sci. **34**, 1547–1562 (2023). https://doi.org/10.1007/s10876-022-02335-1
74. T. Lu and F. Chen, J. Phys. Chem. A **117**, 3100–3108 (2013). https://doi.org/10.1021/jp4010345
75. X. Wang, X. Zhang, W. Pedrycz, et al., Fractal Fract. **8**, 523 (2024). https://doi.org/10.3390/fractalfract8090523
76. F. Mollaamin and M. Monajjemi, Energy Storage **7**, e70122 (2025). https://doi.org/10.1002/est2.70122